Available online at www.sciencedirect.com
SCIENCE DIRECT®
International Journal of Heat and Mass Transfer 47 (2004) 3441–3452
International Journal of HEAT and MASS TRANSFER
www.elsevier.com/locate/ijhmt

Effect of free-stream turbulence on turbine blade heat transfer and pressure coefficients in low Reynolds number flows

Jungho Choi [a], Shuye Teng [a], Je-Chin Han [a,*], Foluso Ladeinde [b]

[a] Turbine Heat Transfer Laboratory, Department of Mechanical Engineering, Texas A&M University, College Station, TX 77843-3123, USA

[b] Department of Mechanical Engineering, SUNY Stony Brook, Stony Brook, NY 11794-2300, USA

Received 19 September 2003; received in revised form 11 January 2004
Available online 20 March 2004

Abstract

The effect of free-stream turbulence on heat transfer and pressure coefficients of a turbine blade was investigated in low Reynolds number flows. Cascade inlet Reynolds number based on blade chord length was varied from 15,700 to 105,000 and turbulence intensity was varied from 0.68% to 15.31%. This study documents the effect of increasing Reynolds number and free-stream turbulence in suppressing separation, promoting boundary layer transition, and enhancing heat transfer on blade surfaces. This may be the first documentation of both the pressure coefficient and Nusselt number distributions on the surfaces of a turbine blade at such low Reynolds numbers. The experimental data are useful for calibrating computational fluid dynamics (CFD) and direct numerical simulation (DNS) codes for predicting turbine blade heat transfer and flow behaviors.

Keywords: Blade heat transfer; Free-stream turbulence; Low Reynolds number

1. Introduction

Flow transition and laminar boundary layer separation in low-pressure turbine blades are attracting increased interest in the industry, due to recent trends such as high altitude flight operations and increased bypass ratios. High-altitude flight operations result in a significant reduction in gas density and thus a decrease of Reynolds number inside a gas turbine engine. Turbine airfoils become very sensitive to flow perturbations and highly prone to flow separation, resulting in poor efficiency and higher localized heat transfer to the blades. Noise regulations have driven more manufacturers to offer engines with higher bypass ratios, reduced core flow and, consequently, lower Reynolds numbers. Reduced Reynolds number operation demands that turbine designers account more carefully for viscous effects, including rapid boundary layer growth, laminar-to-turbulence transition, and boundary layer separation. In addition, a recent tendency to reduce the number of blades and stages in turbo-machines results in more highly loaded blades. A static pressure profile associated with increased surface loading tends to extend the transition region length over a larger fraction of the surface and strengthen separation. All these various effects have led to increased interest in properly understanding boundary layer transition and flow separation under low-pressure turbine conditions.

Many investigator have been addressed the development of boundary layers and separation bubbles in low Reynolds number flows. However, until very recently, most of the literature has focused on boundary layer transition as influenced by infinitesimal

* Corresponding author. Tel.: +1-979-845-3738; fax: +1-979-862-2418.
E-mail address: jchan@mengr.tamu.edu (J.-C. Han).

0017-9310/$ - see front matter
doi:10.1016/j.ijheatmasstransfer.2004.01.015

Nomenclature

C	airfoil chord length, the distance between the leading and trailing edge (0.2268 m)
C_p	pressure coefficient ($=\frac{P_t-P_s}{0.5\rho V_1^2}$)
d	bar width of turbulence grid (m)
h	local heat transfer coefficient (W/m K)
k	thermal conductivity of air at 23 °C (0.02598 W/m K)
Nu	local Nusselt number based on blade chord length and thermal conductivity of air-$=hC/k$
P_t	total pressure at cascade inlet (Pa)
P_{s1}	static pressure at cascade inlet (Pa)
P_s	local static pressure on blade surface (Pa)
q''	local convective heat flux (W/m^2)
q''_{loss}	surface heat loss flux (W/m^2)
q''_{tot}	foil generated surface heat flux (W/m^2)
Re	Reynolds number based on chord length and inlet velocity $=\frac{V_1 C}{v}$
s	distance from turbulence grid to cascade inlet (m)
T_{aw}	local adiabatic wall temperature (°C)
T_w	local surface temperature (°C)
Tu	local turbulence intensity
$V(i)$	local instantaneous velocity (m/s)
$\overline{V}$	local time mean velocity (m/s)
V_1	cascade inlet velocity (m/s)
x	distance from the leading edge to the measuring point along blade surface (m)
v	kinematic viscosity of air (1.5534×10^{-5} m^2/s)
ρ	density of air (1.1766 kg/m^3)

disturbances. Transition in the turbine engine environment, with elevated disturbance levels and periodic unsteadiness, is less well documented. High levels of free-stream turbulence cause earlier transition compared to lower turbulence levels: Such effects can prevent flow separation in the adverse pressure gradient region in the trailing edge portion of the suction surface of a turbine airfoil. Tan and Auld [1] performed hot wire tests on a transitioning and separating turbine cascade in a low-speed wind tunnel at various Reynolds numbers. In their paper, they reported the effects of different boundary layer parameters. Sohn et al. [2] investigated the flow physics occurring on the suction side of a simulated low-pressure turbine (LPT) blade. The experiments were carried out at Reynolds numbers of 100,000 and 250,000 with three levels of free-stream turbulence. Rivir [3] used in an ultra-low Reynolds number cascade environment. They found persistent, massive separation at very low Reynolds numbers (25,000), in spite of elevated free-stream turbulence and added vortices. They also found that elevated free-stream turbulence or added vortices promoted flow reattachment at a higher Reynolds number. Volino and coworkers [4,5] documented boundary layer separation, transition and reattachment under Reynolds number and pressure gradient conditions typical of LPT airfoils. They concluded that Reynolds number and free-stream turbulence level do not have a significant effect on boundary layer separation unless they are high enough to induce transition upstream of separation while the location and extent of the transition zone, in contrast, depend strongly on Reynolds number and turbulence intensity. Van Treuren et al. [6] documented pressure distributions, loss coefficients, and the separation zones in a turbine cascade flow under low Reynolds number (25,000–50,000) conditions. They concluded that massive separation at very low Reynolds numbers (25,000) is persistent, in spite of the elevated free-stream turbulence and added vortices. However, at a higher Reynolds number of 50,000, flow reattachment with elevated free-stream turbulence or with added vortices was eminent. More experimental data on the flow and turbulence quantities in separated boundary layers with reattachment and transition were reported by Qiu and Simon [7] and Hatman and Wang [8,9].

Many studies have investigated the fluid flow and heat transfer behavior in high Reynolds number flows. Blair [10,11] investigated the effect of grid-generated turbulence on flat plate heat transfer. He showed that turbulent heat transfer coefficient in flow with for 6% grid-generated turbulence intensity increased by 18% compared to that without grid. Simonich and Bradshaw [12] and Hancock and Bradshaw [13] reported similar results. O'Brien and VanFossen [14] investigated the influence of jet-grid-generated turbulence on heat transfer from the leading edge of a circular cylinder in crossflow. They reported that for cylinder Reynolds numbers 48,000–180,000, the heat transfer coefficient for a turbulence intensity of 10–12% increases by 37–53% compared to the case with zero turbulence intensity. Bellow and Mayle [15] tested the heat transfer downstream of a leading edge separation bubble on a blunt body. They indicated that the heat transfer through a separation region and for the turbulence intensity of 0.4% increases almost an order of magnitude and is about 50% higher near the reattachment region than is predicted by the turbulent flat plate correlation. Mehendale et al. [16] studied the effect of jet-grid-generated

turbulence on leading edge heat transfer and found an increase of up to 50%. They also found that the inflow turbulence intensity (up to 15%) does not shift the location of the separation–reattachment region. The reattachment heat transfer coefficients are the same despite the inflow turbulence levels and are much higher than the values for the heat transfer coefficient in turbulent flat plate. Brown and Martin [17,18] investigated free-stream turbulence effects on turbine blade heat transfer coefficients. They reported that at gas turbine conditions, the scale and frequency of free-stream turbulence may be as important as its intensity in determining local heat transfer coefficients around the blade. Zhang and Han [19] studied the influence of mainstream turbulence on the surface heat transfer coefficient of a gas turbine blade. Their mainstream Reynolds numbers ranged from 100,000 to 300,000, based on the cascade inlet velocity and blade chord length. Their results showed that mainstream turbulence promoted earlier and broader boundary layer transition, caused higher heat transfer coefficients on the suction surface, and significantly enhanced the heat transfer coefficients on the pressure surface. They also showed that heat transfer coefficient augmentation on the suction surface increases and its peak ratio moves forward with increased mainstream turbulence level. Han et al. [20] studied the effect of unsteady wake on surface heat transfer coefficient of a gas turbine blade using a spoked wheel type wake generator. Their mainstream Reynolds numbers ranged from 100,000 to 300,000. Their results showed that the unsteady passing wake promoted earlier and broader boundary layer transition and caused higher heat transfer coefficients on both the suction surface and pressure surface. Ames [21] investigated the influence of combustor simulated turbulence on turbine vane heat transfer for $Re = 790{,}000$ (based on axial chord). He reported that transition occurred on the suction surface during which the heat transfer level increased rapidly. He also showed a strong effect of turbulence length scale on heat transfer.

As mentioned, flow separation results in higher localized heat transfer in low-pressure turbine blades. However, to the knowledge of the authors, there is no investigation reported in the literature that has taken a close look not only at the flow separation and pressure loss, but also the Nusselt number distributions associated with flow separation in turbine blade cascade at low Reynolds number conditions. The main objective of this study is to provide both pressure coefficient and Nusselt number distributions on the surfaces of a turbine blade at low Reynolds number flows. This study also reports the effect of increasing Reynolds number from 15,700 to 105,000 and free-stream turbulence intensity from 0.6% to 15.31% in suppressing separation, promoting boundary layer transition, and enhancing heat transfer on blade surfaces. The experimental data presented in this paper have been used for calibrating direct numerical simulation (DNS) calculating of turbine blade flow transition and heat transfer [22]. The present study also represents a continuation of Zhang and Han [19] who studied turbine blade heat transfer at higher Reynolds number flows from 100,000 to 300,000.

2. Test apparatus and instrumentation

2.1. Low-speed suction-type wind tunnel

The experiment was performed in a low-speed wind tunnel as shown in Fig. 1 [19]. The wind tunnel consisted of two screens, a contraction nozzle, a five-blade linear cascade, and a blower. The wind tunnel was of the suction type so as to reduce unexpected turbulence intensity in the main stream flow. Two separate stainless steel screens at the inlet of the tunnel ensured that a uniform and parallel flow went into the nozzle. The 4.5:1 contraction nozzle produced a uniform flow entering the test channel. The test channel was 25.4 cm high, 75.0 cm wide in cross-section, and had a 107.49° turn to fit the turning of the five-blade cascade. The width of the test channel was reduced to 35 cm at the cascade outlet to guide the trailing edge parallel flow. The cascade inlet velocity (mainstream Reynolds number) was varied by controlling a sliding gate at the discharge end of a 15 hp (11.2 kW) blower and was continuously monitored by a pitot probe located inside the wind tunnel. A central air-conditioning system maintained the cascade inlet temperature at 25 °C.

2.2. Linear cascade arrangement

The linear test cascade consisted of five blades made of high-quality model wood (RAN SHAPE). The blade configuration was scaled up by a factor of 5 to produce a velocity ratio distribution similar to that inside a typical advanced turbine–blade row. The blades had a chord length of 22.68 cm, a radial span of 25.4 cm, and a blade spacing of 17.01 cm. The blade in the middle of the cascade was the test blade and was instrumented as either a pressure tap or a heat transfer blade, to measure the surface pressure and heat transfer distributions. The details of the blade geometry are not provided here. But the interested reader can either contact the corresponding author for the details or digitize directly from the true geometry shown in Fig. 1.

2.3. Turbulence measurements

A calibrated hot-film probe was used to measure turbulence intensity around the middle test blade. The

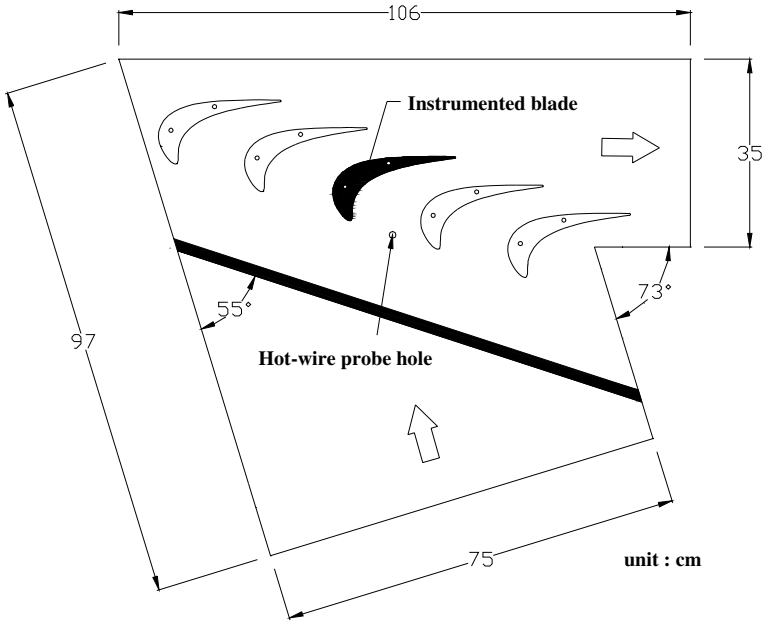

Fig. 1. Test section profile.

probe was connected to a TSI IFA 100 Intelligent Flow Analyzer. The IFA 100 was connected to TSI IFA 200 digitizer, which was interfaced with a PC through an A/D converter. The sample frequency was 50 kHz and the sample size was 10,000. The local time mean velocity and turbulence intensity were calculated as

$$\overline{V} = \frac{1}{N}\sum_{i=1}^{N} V(i)$$

$$Tu = \frac{\sqrt{\sum_{i=1}^{N}(V(i)-\overline{V})^2/(N-1)}}{\overline{V}}$$

where N is the total number of samples.

Fig. 2 shows two types of turbulence grids used to create different levels of turbulence intensity. The coarse grid, shown in Fig. 2(a), was designed to generate higher turbulence intensities. It was made of steel square tubes with a diameter of 1.3 cm and a pitch of 4.8 cm. The fine grid, shown in Fig. 2(b), was designed to generate lower turbulence intensities. It was made of steel square bars with a diameter of 0.5 cm and a pitch of 1.9 cm. Fifty-four percent (54%) of each grid was an open space for air flow. The grids were placed upstream of, and parallel, to the leading edge plane of the blade cascade. Two grid locations were selected in this study, i.e., 21 cm (position #1) and 60 cm (position #2) from the cascade leading edge. s/d is 16, 46 for the coarse grid and is 42 and 120 for the fine grid, respectively. Fig. 3 shows the four different s/d locations and their corresponding turbulence intensities measured at the cascade inlet for each of the four Reynolds numbers. The grid-generated turbulence decreases as s/d increases but increases as Reynolds number increases. For example, the turbulence intensity varied from 8.65% to 15.31% for grid #1 at position #1 as Reynolds number was varied from 15,700 to 105,000.

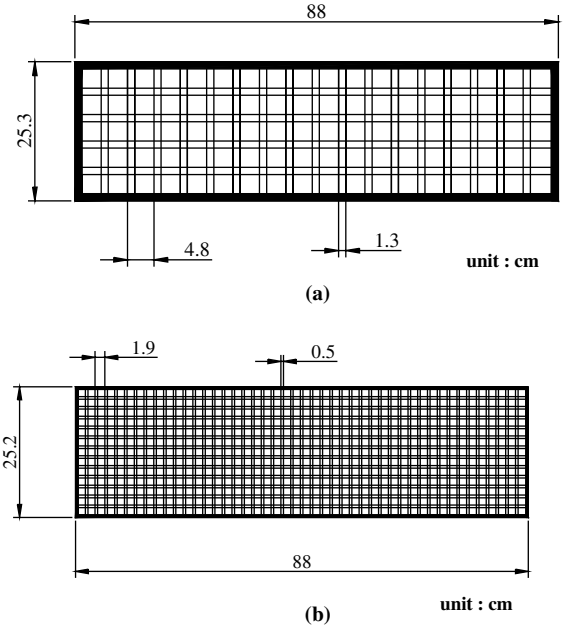

Fig. 2. Turbulence Grid: (a) coarse grid, and (b) fine grid.

Grid	Location (Cm)	Tu(%)			
		Re = 105,000 V=6.94 m/s	Re = 52,000 V=3.44m/s	Re = 31,400 V=2.08 m/s	Re = 15,700 V=1.04m/s
No Grid		0.71	0.73	0.7	0.68
Grid #1	60	5.34	5.02	3.59	2.81
	21	15.31	14.33	10.07	8.65
grid #2	60	2.72	2.6	2.07	1.6
	21	6.76	5.51	4.02	3.08

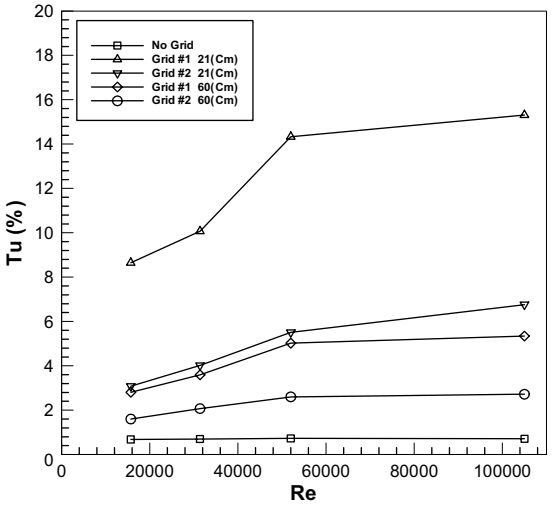

Fig. 3. Turbulence intensity at different *Re*.

2.4. Pressure and velocity measurements

Twenty-six pressure taps were instrumented in the mid-span of a test blade to measure the pressure and velocity distributions around the blade [19]. There was one pressure tap at the leading edge (stagnation point), 11 on the pressure side and 14 on the suction side of the blade. The pressure taps were connected to micromanometer to measure the blade surface static pressure. The micromanometer had an accuracy of 0.00025 inches of water. A pitot probe also measured mainstream flow velocity at the inlet and exit of the cascade. Pressure measurements were expressed as pressure coefficient:

$$C_p = \frac{P_t - P_s}{0.5\rho V_1^2} = \frac{(P_t - P_{s1}) - (P_s - P_{s1})}{P_t - P_{s1}}$$

where P_t is the total pressure of the mainstream flow at the cascade inlet. P_{s1} and P_s are the static pressure at cascade inlet and local static pressure on blade surface. The total pressure is different at each location due to pressure loss along the blade surface. The numerator of the above equation equals to the sum of the dynamic pressure at cascade inlet and the pressure loss of a point on the blade surface. At a given Reynolds number, a higher pressure coefficient compares to higher pressure loss. For the four Reynolds numbers tested in this study, the maximum uncertainty in C_p, shown in Table 1, was estimated to be less than 4.2% (6.54%) for the suction (pressure) side. However, the uncertainty could be much higher (around 50%) in regions very close to the leading edge at a very low Reynolds number (15,700). However, the high uncertainty for C_p happened only near the leading edge region for the lowest Reynolds at 15,700. This is mainly due to very low C_p values occurred near the blade leading edge region. It is obviously that the C_p uncertainty would go up if the measured C_p values go down.

2.5. Measurement of heat transfer coefficient

Fig. 4 shows a test blade instrumented with thin foil heaters to provide constant heat flux on the blade surface and thermocouples to measure the surface heat transfer coefficients. Twenty-six stainless steel strips were vertically cemented on the outer surface of the instrumented blade [19]. Each foil strip was 25.4 cm long, 1.75 cm width, and 0.038 mm thick. All the thin foils were connected in series by copper bus bars. Note that the tiny gaps between the thin foil strips were flushed with glue, no apparent steps between the thin foil strips could be observed from the blade outer surface. The thin foil strips produces as a constant heat flux condition on the blade surface by maintaining a constant voltage in the circuit. A Fluke digital multi-meter measured the voltage and resistance in the circuit to calculate the heat flux of the foil strips. A T-type thermocouple was soldered at each of three different locations in mid-span portion of each foil. All thermocouple output data were analyzed by a Fluke data logger and a PC and were

Table 1
Maximum uncertainties for Nusselt number and pressure coefficient measurements

Re	Nu(%)		C_p (%)		
	Leading edge only ($x/C = 0.077$)	Except leading edge	Pressure side	Suction side	Leading edge
105,000	9.8	3.92	3.54	3.54	3.54
52,000	9.4	3.03	3.75	3.54	4
31,400	8.23	3.5	6.54	3.56	8.7
15,700	9.1	3.6	31.4	4.2	62.6

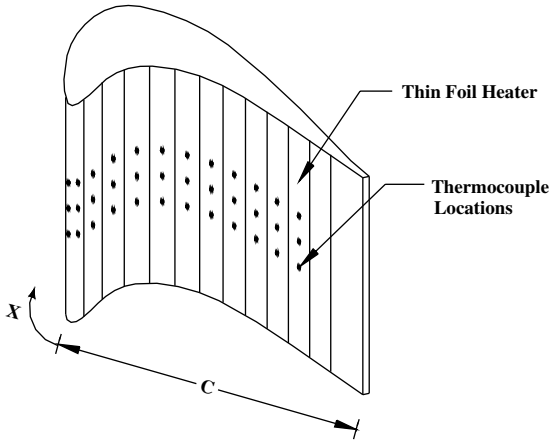

Fig. 4. Heat transfer blade.

averaged at each x/C location. Local heat transfer coefficient is calculated as

$$h = \frac{q''}{T_w - T_\infty} = \frac{q''_{tot} - q''_{loss}}{T_w - T_{aw}}$$

where q'' is the local convective heat flux from the foil surface, q''_{tot} is the total heat flux from the foil heater, and q''_{loss}, affected by conduction, natural convection and radiation, is the local heat loss, which is a function of the difference between the wall temperature (T_w) and the adiabatic wall temperature (T_{aw}). The local adiabatic wall temperature (T_{aw}) was measured at the same Reynolds number condition but without any heat input. T_w was in the 40–50 °C range while T_{aw} was about 25 °C. The local heat transfer coefficient was converted into the local Nusselt number, $Nu = hC/k$, where C is the blade chord length and k is air thermal conductivity. Heat loss tests were conducted for the test blade at no-flow condition. Heat loss was calibrated by supplying power to the test blade at steady state. Several different power inputs were tested to obtain the correlation between the total heat loss and the individual foil temperature. Local radiation loss was estimated using a foil emissivity of 0.22 at the local wall temperature of 45 °C. Conduction loss was estimated based on the blade conductivity and local wall temperature. Heat loss through the tiny thermocouple wires was less than 0.1%, and axial and lateral conduction through the thin foil was found to be negligible. Depending on the location on the surface and surface temperature, the measured total heat loss varies from 7% to 52% of the foil-generated heat. Table 1 gives the maximum uncertainties for Nusselt numbers and pressure coefficients under different test conditions. For the four Reynolds numbers tested in this study, the maximum uncertainty for Nusselt number is between 8.23% and 9.8% for the leading edge and is less than 3.92% for areas other than the leading edge.

3. Results and discussion

3.1. Pressure coefficient distribution on the blade

The periodicity of the velocity profiles between adjacent flow paths and the velocity profiles in the radial direction at the inlet and outlet of the central flow path and at the inlet and outlet of an adjacent flow path have been obtained [19]. The results indicated that the periodicity of velocity profile between adjacent flow paths was excellent and the flow direction at the inlet and outlet of both flow paths was uniform. Also, the inlet and outlet velocity profile was essentially uniform between a 25% and 75% span.

3.2. Effects of Reynolds number

In Fig. 5(a), the local pressure coefficients (C_p) for four Reynolds numbers without grid turbulence are presented to show the effect of Reynolds number on local pressure coefficient. The local pressure coefficient is presented as a function of the normalized distance (x/C) from the leading edge along the blade surface to a local position. On the suction surface, the local pressure coefficient increases along the streamwise direction until $x/C \cong 0.7$, indicating flow acceleration at the upstream portion of the suction surface. The peak at $x/C \cong 0.7$ corresponds to the highest velocity on the suction surface. The local pressure coefficient slightly decreases after the peak, until $x/C \cong 1$, at which point the flow begins to separate. At a given location on the suction surface, the local pressure coefficient increases as Reynolds number decreases. The difference between the two pressure coefficient curves, each corresponding to a different Reynolds number, increases as x/C increases. The effect of Reynolds number on local pressure coefficient becomes negligible when the Reynolds number is reduced to 30,000. On the pressure surface, there is a region of low-velocity flow near the leading edge. The local pressure coefficient remains low and quite stable in the upstream portion ($x/C < 0.4$), and slightly increases as the mainstream flows downstream and starts to accelerate. The local pressure coefficient on the pressure surface decreases with decreasing Reynolds number from 105,000 to 52,000. However, the reverse is true for $x/C > 0.6$. The effect of Reynolds number on local pressure coefficient on the pressure surface is small when Reynolds number is lower than 52,000.

Fig. 5(b)–(e) presents the local pressure coefficient at different Reynolds numbers for the four grid cases, i.e., fine and coarse grids at position #1 (21 cm upstream) and position #2 (60 cm upstream). The effect of Reynolds number on local pressure coefficient for all four grid cases is similar to that for the no-grid case. There is, at a given location on the suction surface, the lower the

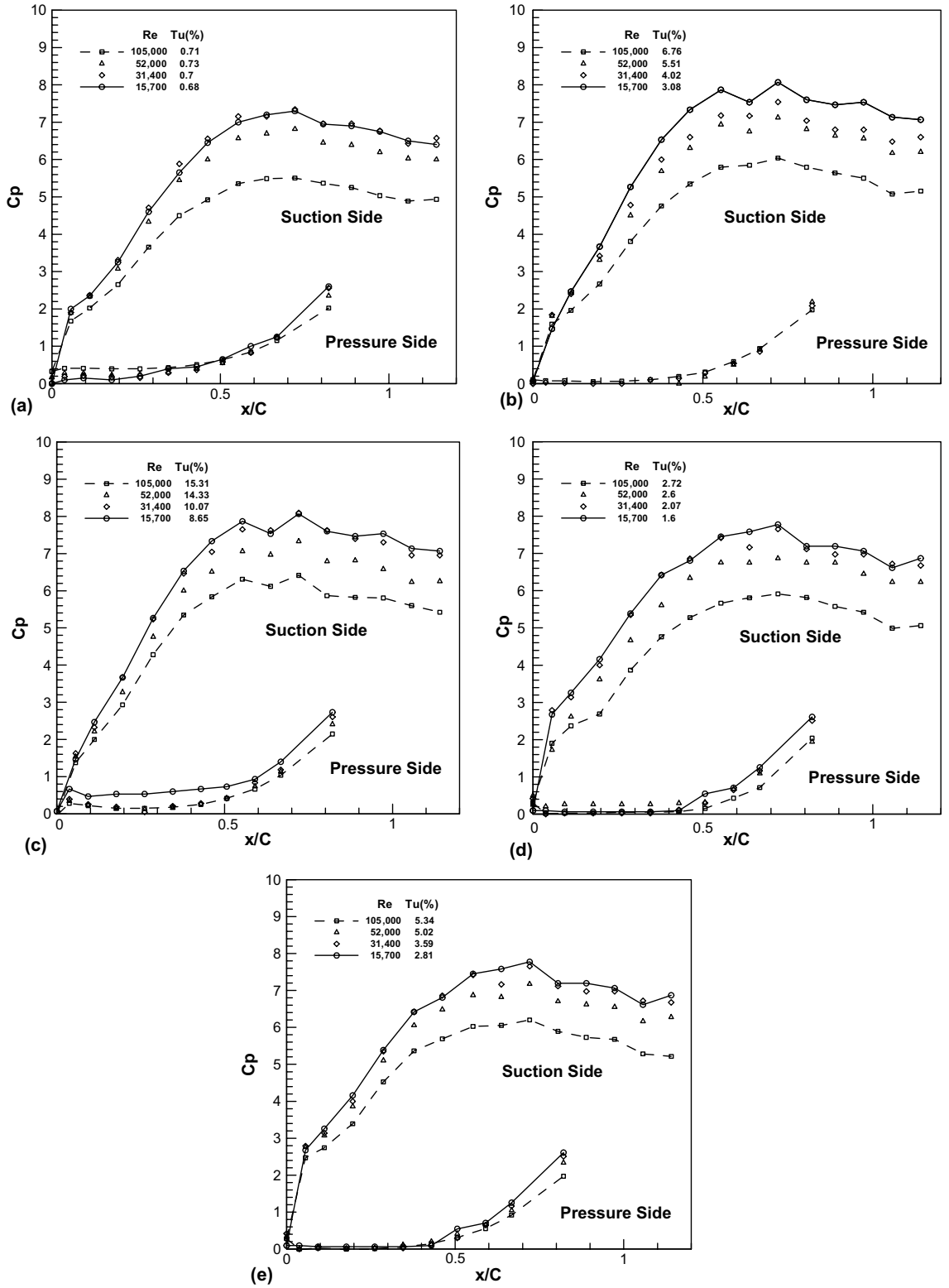

Fig. 5. Effect of Reynolds number on local pressure coefficient distribution: (a) the no grid case, (b) the fine grid at position #1, (c) the fine grid at position #2, (d) the coarse grid at position #1, and (e) the coarse grid at position #2.

Reynolds number, the higher the local pressure coefficient. For the two cases with comparatively low turbulence intensity (fine and coarse grids at position #2), the effect of Reynolds number on local pressure coefficient becomes negligible when the Reynolds number is reduced to 30,000. However, on the pressure surface, local pressure coefficient trends to increase with decreasing Reynolds number.

3.3. Effects of turbulence intensity

Fig. 6(a)–(d) shows the effects of turbulence intensity on the local pressure coefficient at a given Reynolds number. In the $Re = 105{,}000$ case shown in Fig. 6(a), the local pressure coefficient on the suction surface increases as turbulence intensity increases, indicating that higher turbulence intensity results in higher pressure loss. Interestingly, for intensities of about the same value, the coarse grid-generated turbulence intensity (5.34%) has a stronger effect on the local pressure coefficient than does the fine grid-generated turbulence intensity (6.67%). This suggests that turbulence length scale might affect pressure loss. Also, the turbulence intensity effect tends to level off when the turbulence intensity reaches certain high values as shown in Fig. 6(a). On the pressure side, the local pressure coefficient decreases as turbulence intensity increases because higher turbulence intensity impedes flow separation near the leading edge. Fig. 6(b)–(d) shows the effects of turbulence intensity on local pressure coefficient at $Re = 52{,}000$, 31,400, and 15,700, respectively. The same trend is observed from both Fig. 6(b)–(d) as from Fig. 6(a), but the effect of turbulence intensity on local pressure coefficient decreases as Reynolds number decreases.

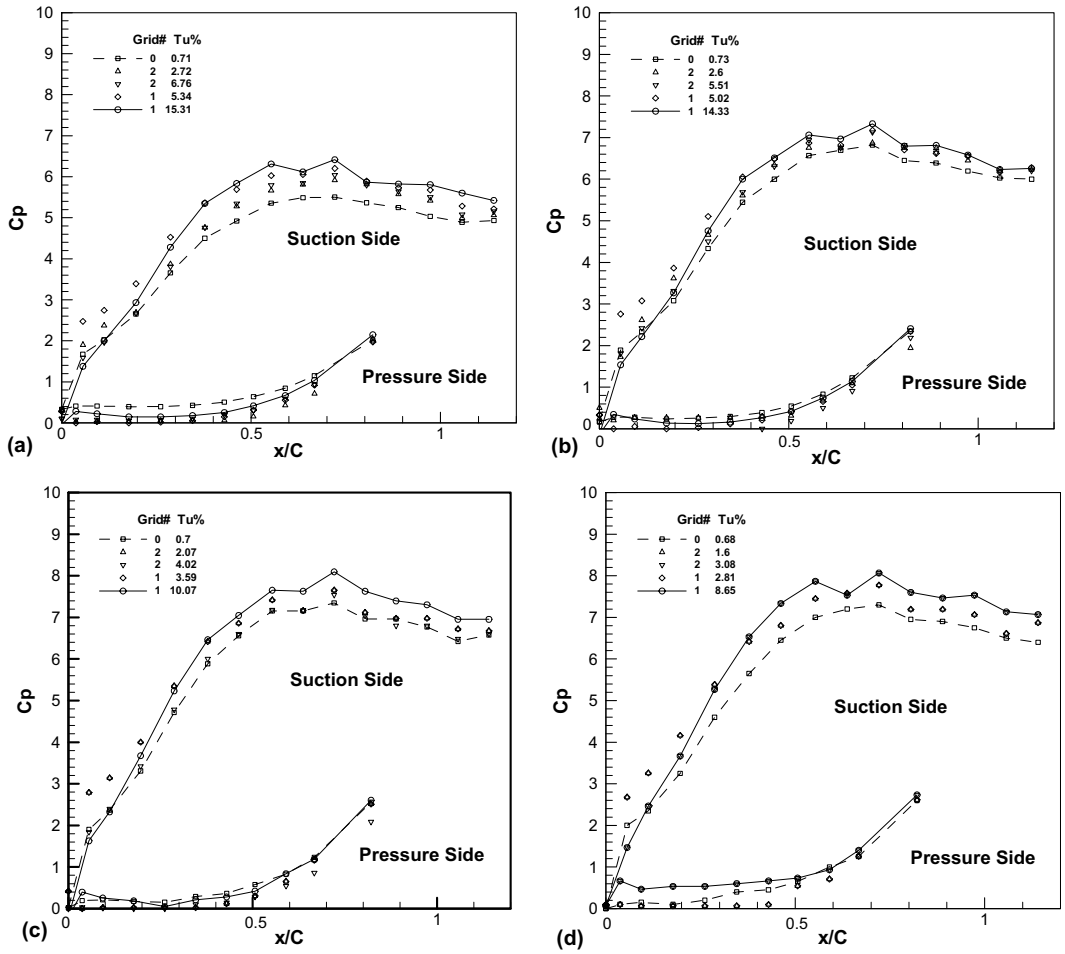

Fig. 6. Effect of turbulence intensity on local pressure coefficient distribution: (a) $Re = 105{,}000$, (b) $Re = 52{,}000$, (c) $Re = 31{,}400$, and (d) $Re = 15{,}700$.

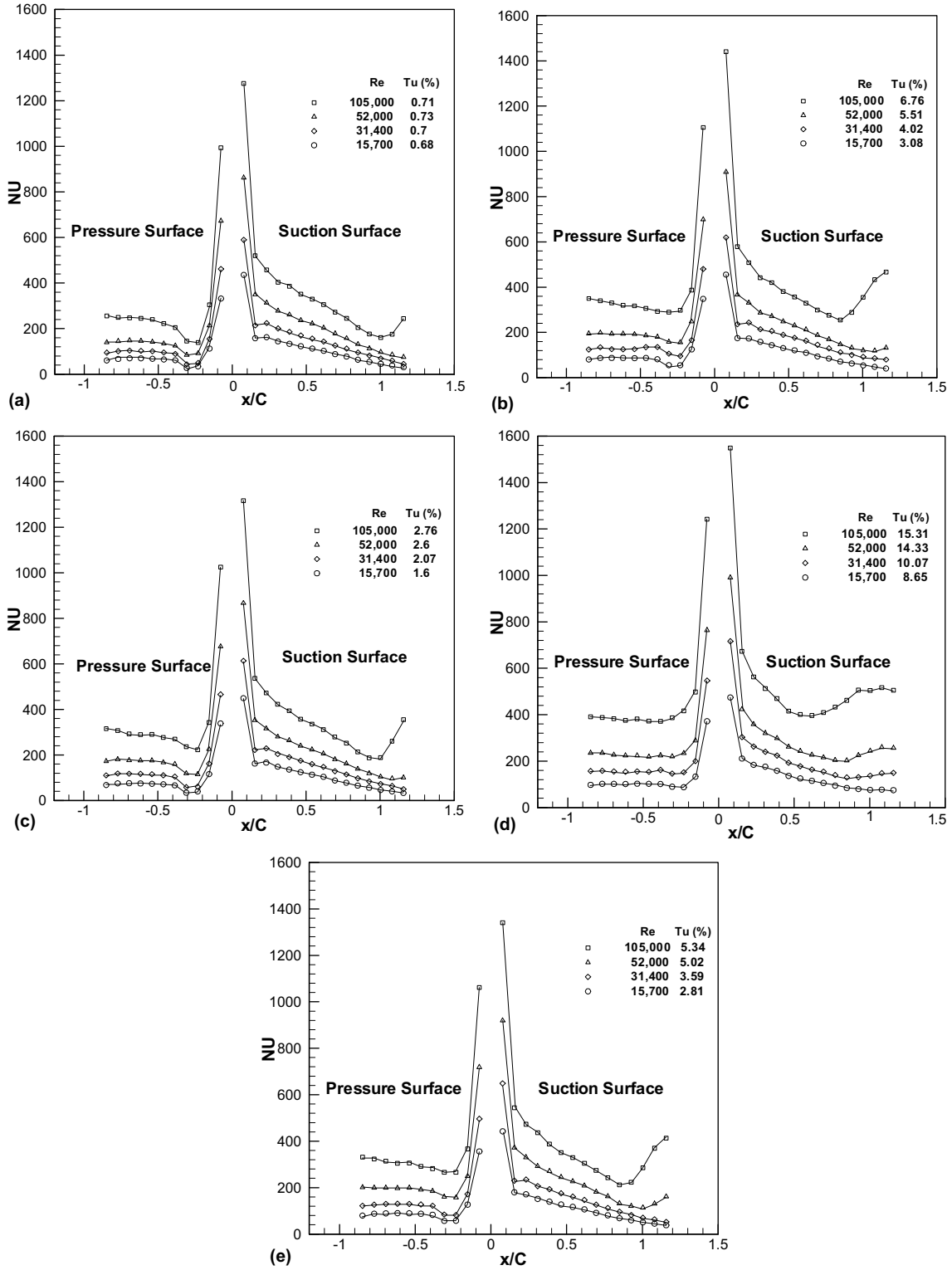

Fig. 7. Effect of Reynolds number on local Nusselt number distribution: (a) the no grid case, (b) the fine grid at position #1 (21 cm upstream), (c) the fine grid at position #2 (60 cm upstream), (d) the coarse grid at position #1 (21 cm upstream), and (e) the coarse grid at position #2 (60 cm upstream).

4. Heat transfer coefficient on the blade

4.1. Effects of Reynolds number

Fig. 7(a) presents the effect of Reynolds number on local Nusselt number distribution for the case without a turbulence grid. The positive and negative abscissa (x/C) indicates the streamwise distance along suction surface and pressure surface, respectively. On the suction surface, the Nusselt number decreases monotonically with increasing streamwise distance due to laminar boundary layer growth. At a given location, the Nusselt number increases as Reynolds number increases. Increasing Reynolds number tends to suppress flow separation on the suction surface. For the low Reynolds number case ($Re = 31{,}400$ and 15,700), a small drop in Nusselt number is observed at $x/C \cong 0.17$ due to the flow separation, while Nusselt number decreases monotonically with increasing streamwise distance for ($Re =$ 52,000 and 105,000). Increasing Reynolds number also promotes boundary layer transition on the suction surface: in the case of high Reynolds number ($Re =$ 105,000), the Nusselt number increases sharply at $x/C \cong 1.0$ due to laminar-to-turbulence transition. On the pressure surface, the Nusselt number decreases sharply with increasing streamwise distance from the leading edge due to laminar boundary layer growth, with lower velocity, with further decrease near $x/C \cong -0.25$ due to a strong flow separation in that region. However, it gradually increases from $x/C < -0.25$ as the flow reattaches and accelerates to impede the laminar boundary layer growth. The Nusselt number on the pressure surface increases as Reynolds number increases.

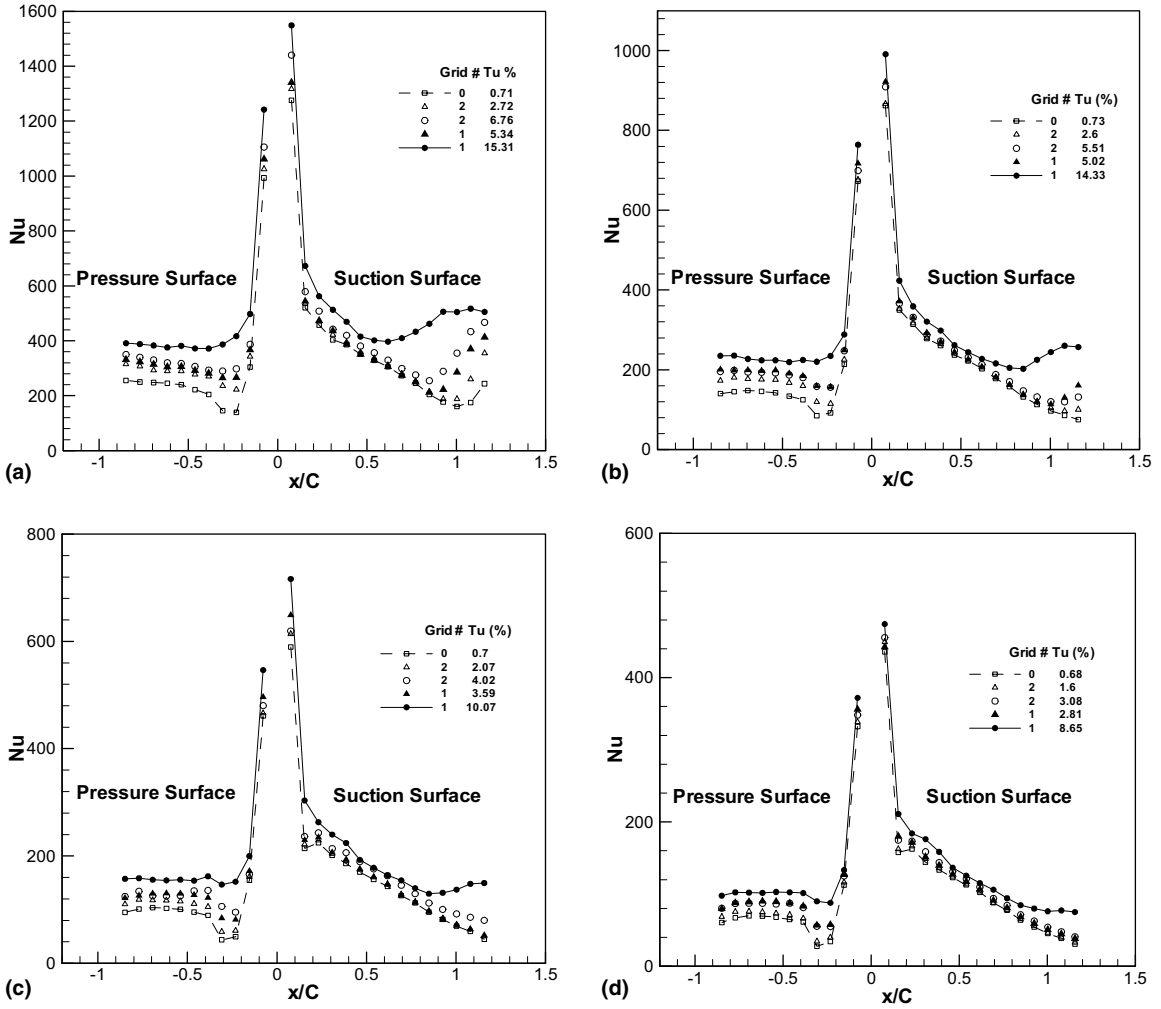

Fig. 8. Effect of turbulence intensity on local nusselt number distribution: (a) $Re = 105{,}000$, (b) $Re = 52{,}000$, (c) $Re = 31{,}400$, and (d) $Re = 15{,}700$.

Fig. 7(b)–(e) respectively presents the effect of Reynolds number on the surface distribution of the local Nusselt number for the fine grid case at position #2 (60 cm upstream), the fine grid case at position #1 (21 cm upstream), the coarse grid case at position #2 (60 cm upstream), and the coarse grid case at position #1 (21 cm upstream). For all the four grid (turbulence) arrangements, the local Nusselt number at a given location increases with increasing Reynolds number.

For low Reynolds numbers ($Re = 31{,}400$ and 15,700), a small drop in Nusselt number due to the flow separation is observed near the suction leading edge for the low Tu cases shown in Fig. 7(c)–(e), indicating that low Reynolds number and low turbulence intensity enhance flow separation near the leading edge. For the high Reynolds number cases ($Re = 52{,}000$ and 105,000), and in all the four grid arrangements, Nusselt number increases sharply downstream on the suction surface due to boundary layer transition. In addition, as shown in Fig. 7(d), boundary layer transition occurs at $x/C \cong 0.5$ for $Re = 105{,}000$, at $x/C \cong 0.8$ for $Re = 52{,}000$. No transition was observed for $Re = 15{,}700$. These observations suggest that high Reynolds numbers promote boundary layer transition. On the pressure surface, for the low Reynolds numbers ($15{,}700 \leqslant Re \leqslant 52{,}000$), Nusselt number decreases sharply due to lower velocity and a strong flow separation upstream at the leading edge, but starts to gradually increase as the flow reattaches and accelerates. Flow separation on the upstream pressure surface is greatly diminished for the cases with higher Reynolds number ($Re = 105{,}000$) and higher Tu (>5%).

4.2. Effect of turbulence intensity

Fig. 8(a)–(d) shows the effects of free-stream turbulence intensity on blade heat transfer for $Re = 105{,}000$, 52,000, 31,400, and 15,700. Overall, at a given Reynolds number, the local Nusselt number increases with increasing turbulence intensity on both the suction and pressure surface.

On the suction surface, an increase in turbulence intensity results in higher heat transfer coefficients. Three explanations can be advanced. Firstly, increasing turbulence intensity promotes earlier boundary layer transition and causes broader boundary layer transition region. For example, for $Re = 105{,}000$, boundary layer transition starts at $x/C \cong 1$ when $Tu = 0.71\%$, but it starts at $x/C \cong 0.5$ when $Tu = 15.31\%$ (Fig. 8(a)). Secondly, an increase in turbulence intensity retards flow separation (low Nusselt number) near the leading edge for low Reynolds number cases ($Re = 31{,}400$ and 15,700) shown in Fig. 8(c) and (d). Thirdly, increasing turbulence intensity disturbs laminar boundary layer regions and thus enhances their heat transfer coefficients.

On the pressure surface, results clearly show that, for $Re = 52{,}000$ and 105,000, high turbulence intensity impedes flow separation near the leading edge and thus eliminates the separation (low Nusselt number) zone in the upstream portion of the pressure surface. The effect of turbulence intensity on flow separation is somewhat reduced for low Re cases such as $Re = 31{,}400$ and 15,700. In general, pressure surface heat transfer coefficients increase with the increase in free-stream turbulence intensity for all Reynolds numbers studied.

5. Conclusions

The influence of free-stream turbulence and inlet Reynolds number ($15{,}700 \leqslant Re \leqslant 105{,}000$) on turbine blade surface pressure coefficient and heat transfer has been investigated in a low-speed wind tunnel. Two different grids were used to generate different turbulence intensity levels. The main conclusions are as follows:

1. In general, local pressure coefficients on both the suction and pressure surfaces increase with decreasing Reynolds number. The effect of Reynolds number on local pressure coefficient becomes negligible when Reynolds number is reduced to 30,000.
2. In general, local pressure coefficients increase on the suction surface and decrease on the pressure surface as the turbulence intensity increases.
3. Flow separation in the leading edge region of the blade is enhanced by decreasing Reynolds number but suppressed as the turbulence intensity increases.
4. Local Nusselt number increases with increasing Reynolds number and increasing turbulence intensity. Also, the local Nusselt number in the separation region near the leading edge decreases with decreasing Reynolds number, but increases as the turbulence intensity increases.
5. Increasing Reynolds number and turbulence intensity tend to promote boundary layer transition and enhance local heat transfer coefficient.

Acknowledgements

The project was supported by the United States National Science Foundation (NSF) under grant number CTS-9903972.

References

[1] A.C.N. Tan, D.J. Auld, Experimental investigations of laminar to turbulent boundary layer transition with separation bubbles at low Reynolds numbers, in: Proceedings

Boundary Layer Transition and Control, Cambridge, UK, April 8–12, 1991.
[2] K.H. Sohn, R.J. Shyne, K.J. DeWitt, Experimental investigation of boundary layer behavior in a simulated low pressure turbine, ASME Paper 98-GT-34, 1998.
[3] R.B. Rivir, Transition on turbine blade and cascade at low Reynolds numbers, in: AIAA 96-2079, 27th AIAA Fluid Dynamics Conference, June 17–20, New Orleans, LA, 1996.
[4] R.J. Volino, L.S. Hultgren, Measurements in separated and transitional boundary layers under low-pressure turbine airfoil conditions, ASME Paper 2000-GT-0260, 2000.
[5] R.J. Volino, C.G., Murawski, Separated flow transition in a low-pressure turbine cascade—mean flow and turbulence spectra, ASME Paper 2003-GT-38727, 2003.
[6] K.W. Van Treuren, T. Simon, M.V. Koller, A.R. Byerley, J.W. Baughn, R. Rivir, Measurements in a turbine cascade flow under ultra low Reynolds number conditions, in: ASME 2001-GT-0164, ASME Turboexpo 2001, June 4–7, New Orleans, LA, 2001.
[7] S. Qiu, W. Simon, An experimental investigation of transition as applied to low pressure turbine suction surface flows, ASME Paper 97-GT-455, 1997.
[8] A. Hatman, T. Wang, Separated flow transition. Part 2—experimental results, ASME Paper 98-GT-462, 1998.
[9] A. Hatman, T. Wang, A prediction model for separated-flow transition, ASME Paper 98-GT-237, 1998.
[10] M.F. Blair, Influence of free-stream turbulence on turbulent boundary layer heat transfer and mean profile development. Part 1—Experimental data, ASME J. Heat Transfer 105 (1983) 33–40.
[11] M.F. Blair, Influence of free-stream turbulence on turbulent boundary layer heat transfer and mean profile development. Part 2—analysis of results, ASME J. Heat Transfer 105 (1983) 41–47.
[12] J.C. Simonich, P. Bradshaw, Effect of free-stream turbulence on heat transfer through a turbulent boundary layer, ASME J. Heat Transfer 100 (1978) 671–677.
[13] P.E. Hancock, P. Bradshaw, Effect of free-stream turbulence on turbulent boundary layer, ASME J. Fluid Eng. 105 (1983) 284–289.
[14] O'J.E. Brien, G.J. VanFossen, The influence of jet-grid turbulence on heat transfer from stagnation region of a cylinder in crossflow, ASME Paper 85-HT-58, 1985.
[15] W.J. Bellow, R.E. Mayle, Heat transfer downstream of a leading edge separation bubble, ASME J. Turbomach. 108 (1986) 131–136.
[16] A.B. Mehendale, J.C. Han, S. Ou, Influence of mainstream turbulence on leading edge heat transfer, ASME J. Heat Transfer 113 (1991) 843–850.
[17] A. Brown, B.W. Martin, Heat transfer to turbine blade, with special reference to the effects of mainstream turbulence, ASME Paper 79-GT-26, 1979.
[18] A. Brown, B.W. Martin, Flow transition phenomena and heat transfer over the pressure surfaces of gas turbine blades, ASME J. Eng. Power 104 (1982) 360–367.
[19] L. Zhang, J.C. Han, Influence of mainstream turbulence on heat transfer coefficients from a gas turbine blade, ASME J. Heat Transfer 116 (1994) 896–903.
[20] J.C. Han, L. Zhang, S. Ou, Influence of unsteady wake on heat transfer coefficient from a gas turbine blade, ASME J. Heat Transfer 115 (1993) 904–911.
[21] F.E. Ames, The influence of large-scale high-intensity turbulence on vane heat transfer, ASME J. Turbomach. 119 (1997) 23–30.
[22] K.A. Alabi, Analysis of the effect of upstream turbulence on aircraft engine turbine blades. Ph.D. Dissertation, Department of Mechanical Engineering, SUNY Stony Brook, Stony Brook, New York, May 2003.